Hindawi
Advances in High Energy Physics
Volume 2024, Article ID 2730568, 19 pages
https://doi.org/10.1155/2024/2730568

Research Article

Properties and Behaviors of Heavy Quarkonia: Insights through Fractional Model and Topological Defects

M. Abu-shady[1] **and H. M. Fath-Allah**[2]

[1]*Department of Mathematics and Computer Sciences, Faculty of Science, Menoufia University, Shibin El Kom, Egypt*
[2]*Higher Institute of Engineering and Technology, Menoufia, Egypt*

Correspondence should be addressed to M. Abu-shady; dr.abushady@gmail.com

Received 2 November 2023; Revised 18 January 2024; Accepted 6 February 2024; Published 2 March 2024

Academic Editor: Shi Hai Dong

In this study, we investigated the impact of a topological defect (λ) on the properties of heavy quarkonia using the extended Cornell potential. We solved the fractional radial Schrödinger equation (SE) using the extended Nikiforov-Uvarov (ENU) method to obtain the eigenvalues of energy, which allowed us to calculate the masses of charmonium and bottomonium. One significant observation was the splitting between nP and nD states, which attributed to the presence of the topological defect. We discovered that the excited states were divided into components corresponding to $2l + 1$, indicating that the gravity field induced by the topological defect interacts with energy levels like the Zeeman effect caused by a magnetic field. Additionally, we derived the wave function and calculated the root-mean radii for charmonium and bottomonium. A comparison with the classical models was performed, resulting in better results being obtained. Furthermore, we investigated the thermodynamic properties of charmonium and bottomonium, determining quantities such as energy, partition function, free energy, mean energy, specific heat, and entropy for P-states. The obtained results were found to be consistent with experimental data and previous works. In conclusion, the fractional model used in this work proved an essential role in understanding the various properties and behaviors of heavy quarkonia in the presence of topological defects.

1. Introduction

The thorough description of hadron properties has become a significant issue in particle and nuclear physics. There have been many attempts to improve chiral quark models to calculate hadron properties, such as [1–5]. Additionally, these models have been extended to quark-gluon plasma in hot or dense mediums, as discussed in [6–8].

By the end of the 1970s, in the existence of grand unification theories (GUT), Kibble predicted that a sequence of spontaneous symmetry breaks would occur in our universe during the cooling phase after the Big Bang [9, 10]. Phase transitions were present in conjunction with these symmetry breaks. According to the Kibble-introduced mechanism, these phase transitions would typically have produced some topological flaws. These flaws are areas of space where energy is concentrated at a very high density. Their spatial dimensions define their natures. These flaws produce the GUT's structure of the collection of empty spaces that the Higgs fields can access. Numerous topological defects, including point defects known as monopoles [9, 11], linear defects or cosmic strings [9, 10, 12], surface defects or domain walls, and combinations of these defects have been examined in the past. Since topological flaws are frequently persistent, it is quite likely that some of them have persisted, possibly even up to the present. Cosmology can detect topological flaws. The dynamics of our universe would be swiftly dominated by monopoles and domain barriers since they are so enormous, which is completely at odds with the observations. Cosmological consequences of cosmic strings could be proven by present and future research, and they are consistent with current observations. The geometry of cosmic strings is flat everywhere except for the symmetry axis, making them the most notable topological defects [9, 11, 13]. They were created early in the universe's history. The variety of theories produced from general relativity theory is a very

strong incentive to investigate how particles behave on these geometrical structures, despite the lack of any fundamental evidence for their existence. The importance of quantum systems in space-times with linear defect geometry should, therefore, receive special attention, as they are thought to constitute the most significant topological flaw in our universe [12]. We can list, for instance, the compression of matter during a moving string's period and temperature variations in the cosmic microwave background (CMB) as key effects of the hypothetical presence of cosmic strings. A cosmic string's gravitational field has peculiar characteristics. A quantum particle at rest near a static, straight line with infinite dimensions would not be drawn to it and would not experience any local gravitational fields as a result. This indicates that close to a cosmic string, space is flat locally [11]. It is not a worldwide flatness, though; it is local. A cosmic string can have a range of effects on quantum particle dynamics because of its particular shape, including the generation or destruction of the (e+, e-) pair [14] and the bremsstrahlung process [15] in the vicinity of a static nucleus. We become interested in the characteristics of hadrons in such spaces under the influence of a central field as a result of these cosmic string-induced fluctuations of quantum observables.

Theoretical high-energy physics (HEP) and related sciences heavily rely on the study of the thermodynamic features of quantum systems [16]. Quarks and gluons typically stay contained in hadrons, especially in the protons and neutrons that make up the atomic nucleus. A plasma of quarks and gluons with poorly understood thermodynamic properties can be produced by compressing or heating nuclei. A theory that explains the strong interaction is called quantum chromodynamics [17, 18]. Several experimental studies have been conducted in recent years to discover the presence of deconfinement transitions [18]. A bound state of charm and anticharm quarks called the $c\bar{c}$, which is suppressed, was then suggested as a potential indicator of the QCD phase change [17, 18]. In-depth research on the thermodynamic characteristics in the case of heavy quarkonia would be intriguing, given that the suppression of the $c\bar{c}$ meson has been identified as the signature of the deconfinement transition. In [19], the authors employed the quark-gluon plasma component quasiparticle model to derive the thermodynamic parameters of the system. Then, utilizing chiral quark models, thermodynamic properties are examined in [20, 21].

With an appropriate transformation, the Schrödinger equation could be transformed into a generalized hypergeometric equation. Consequently, the NU approach can be applied to this type of second-order differential equation with effectiveness. In Ref. [22], a spherically harmonic oscillatory ring-shaped potential is proposed, and its exact complete solutions are presented by the Nikiforov-Uvarov method. As in Ref. [23], the bound states of the Schrödinger equation for a second Pöschl-Teller-like potential are obtained exactly using the Nikiforov-Uvarov method. It is found that the solutions can be explicitly expressed in terms of the Jacobi functions or hypergeometric functions.

In this paper, we derive the SE solutions caused by the gravitational field of a λ for all values of the orbital angular momentum quantum number l_1. The radial Schrödinger equation in the cosmic string background is solved analytically using the generalized fractional extended NU method. Then, we obtain the results to calculate the mass of charmonium and bottomonium, the root-mean radii, and the thermodynamic properties of heavy quarkonia from cosmic string geometry which are not considered in previous works in the framework of fractional nonrelativistic quark models.

This paper is organized as follows: Section 2 reviews the generalized fractional derivative of the ENU method. We obtain the solution for the SE in the cosmic string background for the extended Cornel potential with the generalized fractional derivative of the extended NU method in Section 3. The mass of quarkonia, root-mean radii, and thermodynamic properties of charmonium and bottomonium inside linear defect geometry are described in Section 4. Conclusions are provided in Section 5.

2. The Generalized Fractional Derivative of the Extended Nikiforov-Uvarov (GFD-ENU) Method

ENU method is a generalization of the Nikiforov-Uvarov method. Both are frequently used in quantum physics to determine the eigenvalue and eigenfunctions of the Schrödinger or Dirac equations, as well as any other equations that need to be transformed into a hypergeometric form for a full analysis; for further information, see Refs. [24, 25]. To demonstrate the method viability, the NU was successfully applied in a few practical examples in Ref. [26], where it was generalized to conformable fractional derivative. The goal of this section is to expand the ENU within the confines of the GFD. Take into account the generalized fractional differential equations shown in the standard below [27]:

$$D^{\alpha}[D^{\alpha}[\Psi(x)]] + \frac{\tilde{\tau}(x)}{\sigma(s)} D^{\alpha}[\Psi(x)] + \frac{\tilde{\sigma}(x)}{\sigma^2(x)} \Psi(x) = 0, \tag{1}$$

where $\tilde{\tau}(x)$, $\sigma(x)$, and $\tilde{\sigma}(x)$ are polynomials with degrees of no more than second, third, and fourth, respectively. Then, using GFD [28], we can write

$$D^{\alpha}[\Psi(x)] = \frac{\Gamma(\beta)}{\Gamma(\beta - \alpha - 1)} x^{1-\alpha} \Psi'(x), \tag{2}$$

$$D^{\alpha}[D^{\alpha}[\Psi(x)]] = \left(\frac{\Gamma(\beta)}{\Gamma(\beta - \alpha - 1)} \right)^2 \cdot \left[(1-\alpha) x^{1-2\alpha} \Psi'(x) + x^{2-2\alpha} \Psi''(x) \right], \tag{3}$$

where $0 < \alpha \leq 1$ and $0 < \beta \leq 1$. From Eqs. (2) and (3), we get

$$\Psi''(s) + \frac{\tilde{\tau}(x) + (1-\alpha)x^{1-\alpha}\sigma(x)}{x^{1-\alpha}\sigma(x)}\Psi'(x) + \left(\frac{\Gamma(\beta)}{\Gamma(\beta-\alpha-1)}\right)^{-2}\frac{\tilde{\sigma}(x)}{s^{2-2\alpha}\sigma^2(x)}\Psi(x) = 0. \tag{4}$$

By comparing Eqs. (1) and (4), we get the fractional parameters

$$\tilde{\tau}_f(x) = \tilde{\tau}(x) + (1-\alpha)x^{1-\alpha}\sigma(x),$$
$$\sigma_f(x) = x^{1-\alpha}\sigma(x), \tag{5}$$
$$\tilde{\sigma}_f(x) = \left(\frac{\Gamma(\beta)}{\Gamma(\beta-\alpha-1)}\right)^{-2}\tilde{\sigma}(x).$$

Then, we obtain the standard equation (GFD-ENU):

$$\Psi''(x) + \frac{\tilde{\tau}_f(x)}{\sigma_f(x)}\Psi'(x) + \frac{\tilde{\sigma}_f(x)}{{\sigma_f}^2(x)}\Psi(x) = 0. \tag{6}$$

We assume that the following transforms Eq. (6):

$$\Psi(x) = \Phi(x)Y(x). \tag{7}$$

Eq. (6) is reduced to a hypergeometric equation. Then, we get

$$\sigma_f(x)Y''(x) + \tau_f(x)Y'(x) + \lambda_f(x)Y(x) = 0, \tag{8}$$

where $\Phi(s)$ archive

$$\frac{\Phi'(x)}{\Phi(x)} = \frac{\Pi_f(x)}{\sigma_f(x)}, \tag{9}$$

$$\lambda_f(x) - \Pi_f'(x) = G(x). \tag{10}$$

$Y(x)$ is the hypergeometric function that has a polynomial that archives the Rodrigues relation:

$$Y_n(s) = \frac{B_n}{\rho(x)}\frac{d^n}{ds^n}\left({\sigma^n}_f(x)\,\rho(x)\right), \tag{11}$$

where B_n is the constant for normalization and $\rho(x)$ is the weight function and satisfies the relation

$$\sigma_f'\rho + \rho'\sigma_f = \tau_f\rho. \tag{12}$$

The function $\Pi_f(s)$ is defined as

$$\Pi_f(x) = \frac{\sigma_f'(x) - \tilde{\tau}(x)_f}{2} \pm \sqrt{\left(\frac{\sigma_f'(x) - \tilde{\tau}(x)_f}{2}\right)^2 - \tilde{\sigma}(x) + G(x)\sigma_f(x)}. \tag{13}$$

$\Pi_f(x)$ is a polynomial of at most 2 α degrees, and based on this, the determination of $G(x)$ is important in obtaining $\Pi_f(x)$. $\lambda_n(x)$ is defined by relation

$$\lambda_n(x) = \frac{-n}{2}\tau_f'(x) - \frac{n(n-1)}{6}{\sigma_f}''(x), \tag{14}$$

where

$$\tau_f(x) = \tilde{\tau}(x)_f + 2\,\Pi_f(x). \tag{15}$$

We obtain the eigenvalues of energy from Eq. (10) and Eq. (14).

3. Cosmic String Space-Time of Heavy Quarkonia

In spherical coordinates, the line element that shows the linear defect space-time [10] is obtained by ($x^0 = ct$, $x^1 = r$, $x^2 = \theta$, and $x^3 = \varphi$)

$$ds^2 = \Omega_{\mu\nu}dx^\mu \bigotimes dx^\nu = -c^2\,dt^2 + dr^2 + r^2d\theta^2 + [\chi\,d\theta + \lambda\, r\, \sin\theta\, d\varphi]^2, \tag{16}$$

where $0 < r < \infty$, $0 < \theta < \pi$, $0 < \varphi < 2\pi$, $0 < \lambda = 1 - 4T$ is the topological parameter of the cosmic string, $\chi = 4\,G\,T/c^3$ is the torsion [29] parameter, and T represents the cosmic string's linear mass density. From general relativity (GR), we note that the values of T vary in the interval $T \in]0, 1[$ [29, 30].

For $\lambda \longrightarrow 1$ and $\chi \longrightarrow 0$, the metric obtained by Eq. (16) reduces to the usual Minkowski metric in spherical coordinates [31, 32].

The metric tensor for the space-time given by Eq. (16) is

$$\Omega_{\mu\nu}(x) = \begin{bmatrix} -1 & 0 & 0 & 0 \\ 0 & 1 & 0 & 0 \\ 0 & 0 & \chi^2 + r^2 & \chi\lambda r\, \sin\theta \\ 0 & 0 & \chi\lambda r\, \sin\theta & \lambda^2 r^2\, \sin^2\theta \end{bmatrix} = \begin{bmatrix} -1 & 0 \\ 0 & (\Omega_{ij}) \end{bmatrix}. \tag{17}$$

With the inverse metric,

$$\Omega^{\mu\nu}(x) = \begin{bmatrix} -1 & 0 & 0 & 0 \\ 0 & 1 & 0 & 0 \\ 0 & 0 & \frac{1}{r^2} & \frac{-\chi}{\lambda\, r^3\, \sin\theta} \\ 0 & 0 & \frac{-\chi}{\lambda\, r^3\, \sin\theta} & \frac{\chi^2 + r^2}{\lambda^2 r^4\, \sin^2\theta} \end{bmatrix}. \tag{18}$$

We choose the signature $(-, +, +, +)$ for the metric tensor $\Omega^{\mu\nu}$, and its determinant is obtained by $\Omega = \det(\Omega^{\mu\nu}) = -\lambda^2 r^4\, \sin^2\theta$, with $\mu, \nu = 0, 1, 2, 3$. In the system of curvilinear coordinates $ds^2 = \sum_{i=1}^{3}\sum_{j=1}^{3}\Omega_{ij}\,dx^i \otimes dx^j$ such

that $r \longrightarrow x^1$, $\theta \longrightarrow x^2$, and $\varphi \longrightarrow x^3$, the 3-dimensional interior Euclidian space's metric tensor is

$$\Omega_{ij}(x) = \begin{bmatrix} 1 & 0 & 0 \\ 0 & \chi^2 + r^2 & \chi\lambda r \sin\theta \\ 0 & \chi\lambda r \sin\theta & \lambda^2 r^2 \sin^2\theta \end{bmatrix}. \tag{19}$$

The Laplace-Beltrami (LB) operator of the local coordinate system may be described as

$$\Delta_{\mathrm{LB}} = \frac{1}{\sqrt{\Omega}} \frac{\partial}{\partial x^i} \left(\Omega^{ij} \sqrt{\Omega} \frac{\partial}{\partial x^i} \right) \quad i, j = 1, 2, 3, \Omega = \det\left(\Omega_{ij}\right) = \lambda^2 r^4 \sin^2\theta. \tag{20}$$

Next, considering Equation (20) and for small values of the torsion parameter $\chi \ll 1$, the LB operator is

$$\Delta_{\mathrm{LB}} = \frac{1}{r^2} \left\{ \frac{\partial}{\partial r} \left[r^2 \left(\frac{\partial}{\partial r} \right) \right] + \cot\theta \frac{\partial}{\partial \theta} + \frac{\partial^2}{\partial \theta^2} + \frac{1}{\lambda^2 \sin^2\theta} \frac{\partial^2}{\partial \varphi^2} \right\}. \tag{21}$$

The Hamiltonian operator in natural can be written from this. $(\hbar = c = 1)$ as:

$$H = -\frac{1}{2M} \left[\frac{\partial^2}{\partial r^2} + \frac{2}{r} \frac{\partial}{\partial r} + \frac{1}{r^2} cot\theta \frac{\partial}{\partial \theta} + \frac{1}{r^2} \frac{\partial^2}{\partial \theta^2} + \frac{1}{r^2} \frac{1}{\lambda^2 \sin^2\theta} \frac{\partial^2}{\partial \varphi^2} \right] + V(r, \theta, \varphi). \tag{22}$$

$M = m_q\, m_{\bar{q}}/(m_q + m_{\bar{q}})$ is the reduced mass, where $m_q, m_{\bar{q}}$ are the mass of quark and antiquark [26, 33].

Now, in curved cosmic string space-time, the nonrelativistic radial SE is presented in detail [12, 29].

$$\frac{d^2\psi_{nl}(r)}{dr^2} + \left[-\frac{2M}{\hbar^2} V(r) + \frac{2M}{\hbar^2} E_{nl} - \frac{\delta}{r^2} \right] \psi_{nl}(r) = 0, \tag{23}$$

where $\delta = l_{(\lambda)}(l_{(\lambda)} + 1)$ with $l_{(\lambda)} = m_{(\lambda)} + n$ and the quantum number for generalized angular orbits is $l_{(\lambda)}$. It is not necessarily the case that the generalized quantum numbers $l_{(\lambda)}$ and $m_{(\lambda)}$ are integers: $l_{(\lambda)} = m_{(\lambda)} + n = (m/\lambda) + n = l_1 - (1 - (1/\lambda))m$, where $l_1 = 0, 1, 2, \cdots$.

Suppose two heavy quarks in a bound state like the $c\bar{c}$ and $b\bar{b}$ with the potential consisting of the Cornell potential plus harmonic potential. The linear part is responsible for quark confinement at large distances, while the Coulomb part dominates at short distances. This potential has been extensively studied in both relativistic and nonrelativistic quantum mechanics and has attracted a great deal of attention in particle physics in which the additional part was added to improve confinement force, and we found that it gave a good result compared with other works and experimental results [34].

$$V(r) = ar^2 + br - \frac{c}{r} + d. \tag{24}$$

To put Eq. (23) in the dimensional fractional form, we let $r = y/A$, $M' = M/A$, and $E' = E/A$, where $A = 1\,\mathrm{GeV}$. δ is separation constant $\delta = l_{(\lambda)}(l_{(\lambda)} + 1)$. Then we get

$$D^\alpha[D^\alpha \psi_{nl}(y)] + 2\mu' \left(E' - \frac{V(y)}{A} \right) - \frac{\delta}{z^{2\alpha}} \psi_{nl}(y) = 0, \tag{25}$$

where $a' = a/A^3$, $b' = b/A^2$, $c' = c$, $d' = d/A$, and $\zeta = (\Gamma(\beta))/(\Gamma(\beta - \alpha - 1))$.

By using Eq. (3), we get

$$\psi''_{nl}(y) + \frac{1-\alpha}{z} \psi'_{nl}(y) + \frac{1}{z^2} \left(\left(\varepsilon - d^1 \right) y^{2\alpha} - a^1 y^{4\alpha} - b^1 y^{3\alpha} + c^1 y^\alpha - \delta^1 \right) \psi_{nl}(y) = 0, \tag{26}$$

where $\varepsilon = 2M'E'/\zeta^2$, $a^1 = 2M'a'/\zeta^2$, $b^1 = 2M'b'/\zeta^2$, $c^1 = 2M'c'/\zeta^2$, $d^1 = 2M'd'/\zeta^2$, and $\delta^1 = \delta/\zeta^2$.

$$\psi''_{nl}(y) + \frac{1-\alpha}{z} \psi'_{nl}(y) + \frac{1}{z^2} \left(-\varsigma_1 y^{4\alpha} - \varsigma_2 y^{3\alpha} - \varsigma_3 y^{2\alpha} - \varsigma_4 y^\alpha - \varsigma_5 \right) \psi_{nl}(y) = 0, \tag{27}$$

where $\varsigma_1 = a^1$, $\varsigma_2 = b^1$, $\varsigma_3 = -\varepsilon + d^1$, $\varsigma_4 = -c^1$, and $\varsigma_5 = \delta^1$.

By comparing Eq. (6) and Eq. (27), we get

$$\tilde{\tau} = 1 - \alpha, \sigma_f = y, \tilde{\sigma}_f = -\varsigma_1 y^{4\alpha} - \varsigma_2 y^{3\alpha} - \varsigma_3 y^{2\alpha} - \varsigma_4 y^\alpha - \varsigma_5. \tag{28}$$

Then, we get

$$\Pi_f(y) = \frac{\alpha}{2} \pm \sqrt{\varsigma_1 y^{4\alpha} + \varsigma_2 y^{3\alpha} + \varsigma_3 y^{2\alpha} + \varsigma_4 y^\alpha + \overline{\varsigma_5} + y\, G(y)}, \tag{29}$$

where $\overline{\varsigma_5} = \varsigma_5 + \alpha^2/4$. We choose a linear function $G(y) = A^* y^{2\alpha-1} + B y^{\alpha-1}$ that produces the functions under the root in the above equation to be quadratic $(A_1 y^{2\alpha} + A_2 y^\alpha + A_3)^2$. Then,

$$\Pi_f(y) = \frac{\alpha}{2} \pm \left(A_1 y^{2\alpha} + A_2 y^\alpha + A_3 \right). \tag{30}$$

Table 1: Mass spectra of charmonium (in GeV) for two models (the classical model ($\alpha = \beta = 1$) and the fractional model ($\alpha = 0.84$, $\beta = 1$) at $\lambda = 0.8$).

State	The classical model	The fractional model	[36]	[37]	[38]	[39]	Exp. [42]	Error of the classical model	Error of the fractional model
1S	3.096	3.074	3.078	3.096	3.078	3.239	3.096	0	0.007
2S	3.619	3.582	4.187	3.686	3.581	3.646	3.649	0.008	0.018
3S	4.142	4.090	5.297	3.984	4.085	4.052	4.040	0.025	0.012
4S	4.665	4.598	6.407	4.150	4.589	4.459	4.415	0.056	0.041
1P	3.488	3.513							
	3.619	3.654	3.415	3.433	3.415	3.372	3.525	0.010	0.003
	3.75	3.796							
2P	4.011	4.020							
	4.142	4.163	4.143	3.910	3.917	3.779	3.900	0.005	0.007
	4.273	4.305							
1D	3.358	5.067							
	3.75	4.644							
	3.142	4.221	3.752	3.767	3.749	3.604	3.769	0.028	0.030
	4.534	3.796							
	4.927	3.369							
Total error	0.018	0.016	0.9513	0.11065	0.11152	0.05788	—		

Comparing Eq. (29) and Eq. (30), we obtain

$$\begin{aligned} A_1 &= \pm\sqrt{\varsigma_1}, \\ A_2 &= \pm\frac{\varsigma_2}{2\sqrt{\varsigma_1}}, \\ A_3 &= \pm\sqrt{\overline{\varsigma_5}}, \\ A^* &= \frac{{\varsigma_2}^2}{4\varsigma_1} \pm 2\sqrt{\varsigma_1\overline{\varsigma_5}} - \varsigma_3, \\ B &= \pm\frac{\varsigma_2}{\sqrt{\varsigma_1\overline{\varsigma_5}}} - \varsigma_4, \end{aligned} \tag{31}$$

$$\tau_f(y) = 1 \pm 2\left(A_1 y^{2\alpha} + A_2 y^{\alpha} + A_3\right). \tag{32}$$

From Eq. (10), we obtain

$$\lambda(y) = A^* y^{2\alpha-1} + B y^{\alpha-1} \pm \left(2A_1 y^{2\alpha-1} + \alpha A_2 y^{\alpha-1}\right). \tag{33}$$

From Eq. (14), we obtain

$$\lambda_n(y) = -n\left(\pm 2A_1 y^{2\alpha-1} + \alpha A_2 y^{\alpha-1}\right). \tag{34}$$

We have four different combinations of sign choices ++, +−, −+, and −−. We chose ++ to obtain the eigenvalue of energy and the eigenfunction as in Ref. [26]. We obtain the energy eigenvalue from Eq. (33) and Eq. (34):

$$E_{nlm} = d - \frac{b^2}{4a} + \zeta^2\sqrt{\frac{2a}{M}}\left[(n+1)\alpha + \sqrt{\frac{\alpha^2}{4} + \frac{1}{\zeta^2}\left[l_1 - \left(1 - \frac{1}{\lambda}\right)m\right]\left[l_1 - \left(1 - \frac{1}{\lambda}\right)m + 1\right]}\right]. \tag{35}$$

From Eq. (9), we obtain the function $\Phi(y)$:

$$\Phi(y) = k y^{(\alpha/2)+A_3} e^{(1/2)\left((A_1/\alpha)y^{2\alpha} + (2A_2/\alpha)y^{\alpha-1}\right)}, \tag{36}$$

where A_1, A_2, and A_3 are obtained from Eq. (31). From Eq. (12), we obtain the function $\rho(z)$:

$$\rho(y) = y^{2A_3} e^{\left((A_1/\alpha)y^{2\alpha} + (2A_2/\alpha)y^{\alpha-1}\right)}. \tag{37}$$

Then, we obtain the function $Y_n(s)$:

$$Y_n(s) = B_n y^{-2A_3} e^{-\left((A_1/\alpha)y^{2\alpha} + (2A_2/\alpha)y^{\alpha}\right)} \frac{d^n}{dz^n} \cdot \left[y^{2A_3+n} e^{\left((A_1/\alpha)y^{2\alpha} + (2A_2/\alpha)y^{\alpha-1}\right)}\right]. \tag{38}$$

Table 2: Mass spectra of bottomonium (in GeV) for two models (the classical model ($\alpha = \beta = 1$) at $\lambda = 0.7$ and the fractional model ($\alpha = 0.8$, $\beta = 0.9$) at $\lambda = 0.8$).

State	The classical model	The fractional model	[36]	[38]	[40]	Exp. [43]	Error of the classical model	Error of the fractional model
1S	9.460	9.465	9.510	9.510	9.460	9.460	0	0.0005
2S	9.844	9.853	10.627	10.038	10.023	10.023	0.018	0.016
3S	10.288	10.241	11.726	10.566	10.585	10.355	0.006	0.011
4S	10.611	10.628	12.834	11.094	11.148	10.580	0.003	0.004
1P	9.679 9.843 10.008	9.802 9.911 10.020	9.862	9.862	9.492	9.900	0.006	0.001
2P	10.063 10.228 10.392	10.19 10.299 10.408	10.944	10.390	10.038	10.260	0.003	0.003
1D	9.898 10.063 10.227 10.392 10.557	10.129 10.237 10.345 110.733 11.120	10.214	10.214	9.551	10.161	0.006	0.003
Total error	0.006	0.0055	0.484	0.0137	0.028	—		

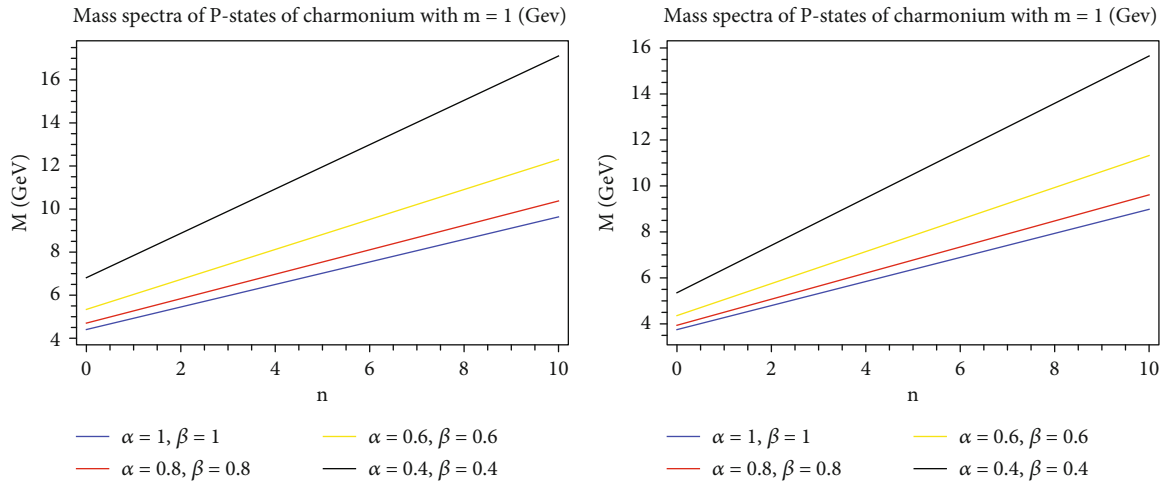

Figure 1: (a) Mass spectrum (in GeV) of charmonium, at various values of α, β, is plotted as a function of quantum number (n) at a topological defect ($\lambda = 0.4$) at $m = +1$. (b) Mass spectrum (in GeV) of charmonium, at various values of α, β, is plotted as a function of n at a topological defect ($\lambda = 0.8$) at $m = +1$.

From Eq. (7), we obtain the fractional radial wave function:

$$\psi_{nl}(y) = N_{nl} y^{(\alpha/2)-A_3}\, e^{-\left((A_1/2\alpha)y^{2\alpha}+(A_2/\alpha)y^{\alpha-1}\right)} \frac{d^n}{dy^n} \cdot \left[y^{2A_3+n} e^{\left((A_1/\alpha)y^{2\alpha}+(2A_2/\alpha)y^{\alpha-1}\right)}\right], \tag{39}$$

where N_{nl} is the normalization constant.

4. Results and Discussions

4.1. Special Cases. The classical case is obtained ($\alpha = \beta = 1$); then, $\zeta = 1$. The eigenvalues of energy and wave function in the classical model are

$$E_{nlm} = d - \frac{b^2}{4a} + \sqrt{\frac{2a}{M}}\left[(n+1) + \sqrt{\frac{1}{4} + \left[l_1 - \left(1 - \frac{1}{\lambda}\right)m\right]\left[l_1 - \left(1 - \frac{1}{\lambda}\right)m + 1\right]}\right],$$
$$\psi_{nl}(y) = N_{nl} y^{(1/2)-A_3} e^{-\left((A_1/2)y^2+A_2\right)} \frac{d^n}{dy^n}\left[y^{2A_3+n} e^{\left(A_1 y^2+2A_2\right)}\right]. \tag{40}$$

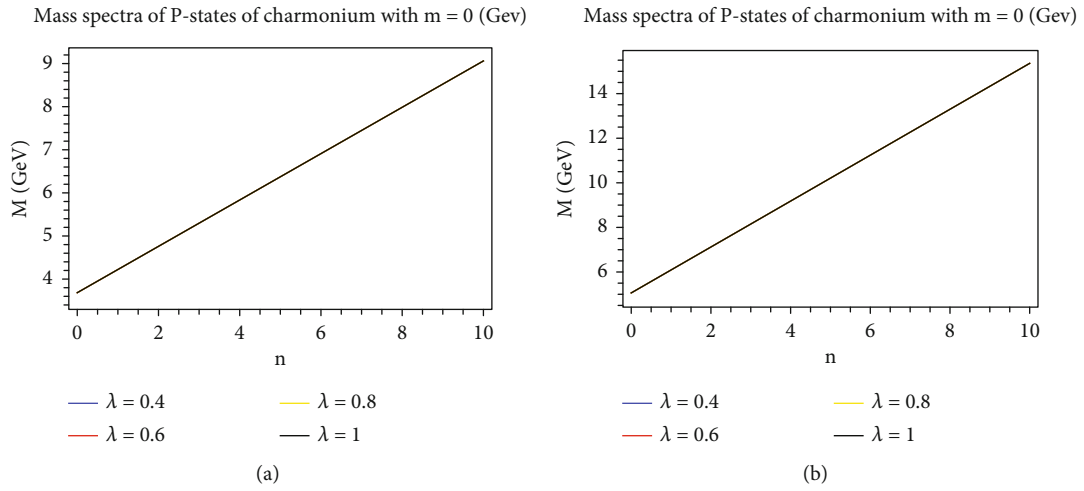

FIGURE 2: (a) Mass spectrum (in GeV) of charmonium is plotted as a function of n at various values of topological defect λ at $\alpha = \beta = 0.9$ at $m = 0$. (b) Mass spectrum (in GeV) of charmonium is plotted as a function of n at various values of topological defect λ with $\alpha = \beta = 0.4$ at $m = 0$.

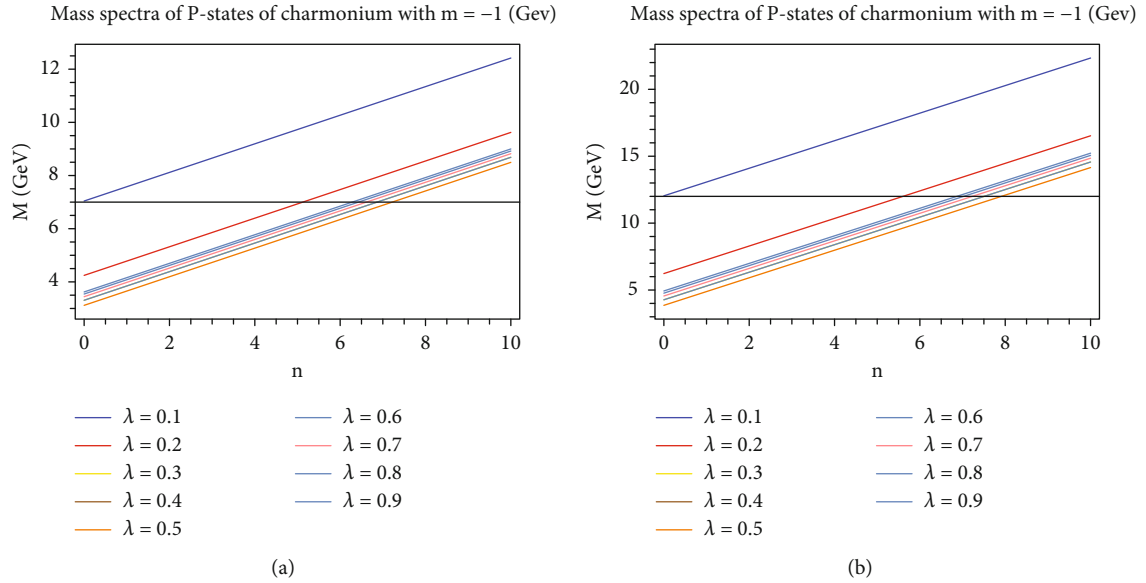

FIGURE 3: (a) Mass spectrum (in GeV) of charmonium is plotted as a function of the quantum number (n) at different values of topological defect λ at $\alpha = \beta = 0.9$ at $m = -1$. (b) Mass spectrum (in GeV) of charmonium of the quantum number n at different values of topological defect λ at $\alpha = \beta = 0.4$ at $m = -1$.

4.2. Mass of Heavy Quarkonia. We obtain the mass of both charmonium and bottomonium from the relation

$$M = m_1 + m_2 + E_{nlm} = m_1 + m_2 + d - \frac{b^2}{4a} + \zeta^2 \sqrt{\frac{2a}{M}}\left[(n+1)\alpha + \sqrt{\frac{\alpha^2}{4} + \frac{1}{\zeta^2}\left[l - \left(1 - \frac{1}{\lambda}\right)m\right]\left[l - \left(1 - \frac{1}{\lambda}\right)m + 1\right]}\right]. \quad (41)$$

In Table 1, the mass of $c\bar{c}$ has been calculated for 1S, 2S, 3S, 4S, 1P, 2P, and 1D for different values of topological defect λ. We have calculated the Schrödinger equation by using the generalized fraction (ENU) method, and we obtained the mass of $c\bar{c}$ under the effect λ. The potential parameters a, b, and d are fitted using Eq. (41) where $a = 0.0826\,\text{GeV}^3$, $b = 0.41849\,\text{GeV}^2$, and $d = 0.427269\,\text{GeV}$, and the quark mass ($m_c = 1.207\,\text{GeV}$) is obtained from Refs. [26, 35]. We obtained the mass of $c\bar{c}$ in two models. The classical model at $\alpha = \beta = 1$ with topological defect ($\lambda = 0.8$). We obtained a good result compared with previous works. In addition, some of the states of charmonium are close with experimental data. We calculated the total error which equals to 0.018% in the classical model. In the fractional model, the total error is smaller than the classical model

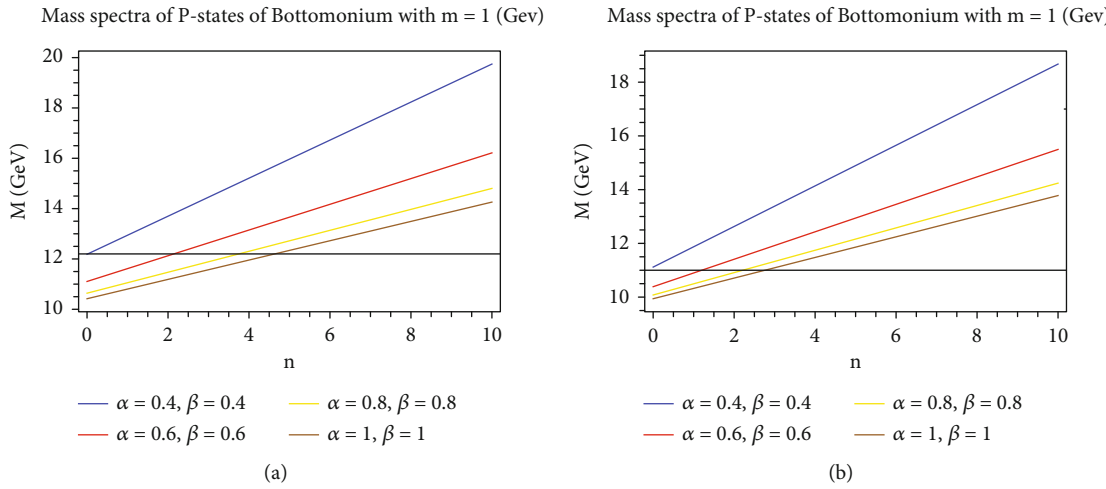

FIGURE 4: (a) Mass spectrum (in GeV) of bottomonium is plotted as a function of n at various values of α, β at a topological defect ($\lambda = 0.4$) at $m = +1$. (b) Mass spectrum (in GeV) of bottomonium is plotted as a function of n at various values of α, β at a topological defect ($\lambda = 0.8$) at $m = +1$.

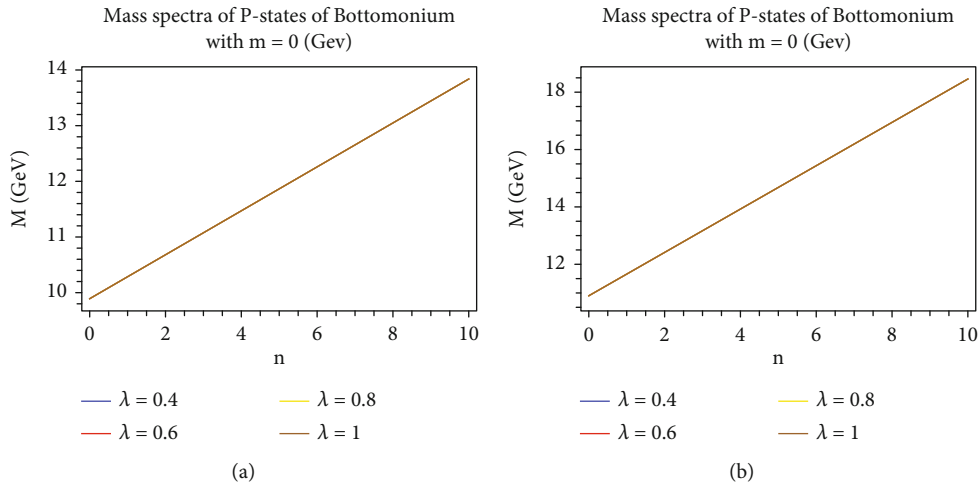

FIGURE 5: (a) Mass spectrum (in GeV) of bottomonium is plotted as a function of n at various values of topological defect λ at $\alpha = \beta = 0.9$ at $m = 0$. (b) Mass spectrum (in GeV) of bottomonium is plotted as a function of n at various values of topological defect λ at $\alpha = \beta = 0.4$ at $m = 0$.

which equals to 0.016%. In the present work, the topological defect parameter takes values between $0 < \lambda < 1$. The topological defect produces a splitting in the mass spectrum of the $c\bar{c}$ meson to break the degeneracy in the nP and nD states, which was absent in earlier studies. In Ref. [36], the authors studied the N-radial Schrödinger equation by using the asymptotic iteration method for the quark-antiquark interaction potential, and they calculated the mass spectra of heavy quarkonia, so we calculated the total error of this work which equals to 0.9513%. In Ref. [37], the authors solved the Schrödinger equation by using the Nikiforov-Uvarov method for the sum of a harmonic, a linear, and a Coulomb interaction potential, and they calculated the mass spectra of heavy quarkonia, so we calculated the total error of this work which equals to 0.11065%. In Ref. [38], the authors calculated the N-radial Schrödinger equation by using the power series iteration method for the quark-antiquark interaction potential, and they calculated the mass spectra of heavy quarkonia, so we calculated the total error of this work that equals to 0.11152%. In Ref. [39], the authors studied the N-radial Schrödinger equation by using an exact analytical iteration method for the trigonometric Rosen-Morse of the quark-antiquark interaction potential, and they calculated the mass spectra of heavy quarkonia in which we found the total error that equals to 0.05788%. Therefore, we obtained improved results in comparison with [36–39].

In Table 2, the mass of $b\bar{b}$ has been calculated for 1S, 2S, 3S, 4S, 1P, 2P, and 1D for different values of topological defect λ. We have calculated the Schrödinger equation by using the generalized fraction ENU method, and we get the mass of $b\bar{b}$ under effect λ. The potential parameters a, b, and d are fitted using Eq. (41), where $a = 0.17776\,\text{GeV}^3$, $b = 0.6898\,\text{GeV}^2$, and $d = -0.0927487\,\text{GeV}$, and the quark

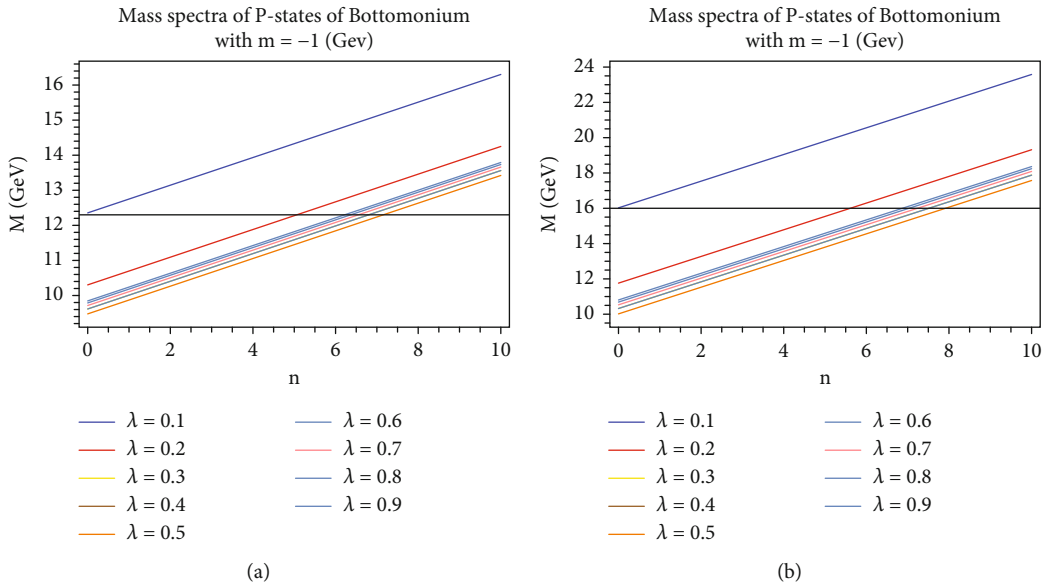

FIGURE 6: (a) Mass spectrum (in GeV) of bottomonium is plotted as a function of n at various values of topological defect λ at $\alpha = \beta = 0.9$ at $m = -1$. (b) Mass spectra (in GeV) of bottomonium is plotted as a function of n at various values of topological defect λ at $\alpha = \beta = 0.4$ at $m = -1$.

TABLE 3: The expectation value of charmonium of $\langle y \rangle$ $((\text{GeV})^{-1})$ for two models (the classical model ($\alpha = \beta = 1$, $\lambda = 0.1$), the fractional model ($\alpha = 0.6$, $\beta = 0.27$, $\lambda = 0.9$)).

State	The classical model $\langle y \rangle$ $((\text{GeV})^{-1})$	The fractional model $\langle y \rangle$ $((\text{GeV})^{-1})$	[44]	[44]	[45]	[46]	[47]
1S	1.184	3.030	3.073	3.086	2.619	2.790	1.002
2S	1.601	4.732	5.770	5.777	4.761	4.612	1.551
	4.170	3.554					
1P	1.545	3.664	4.331	4.325	—	4.266	—
	4.722	3.779					
	4.347	5.231					
2P	1.894	5.337	7.511	7.488	3.725	5.588	—
	4.883	5.447					
	6.137	4.529					
	3.873	4.660					
1D	2.025	4.792	6.410	6.380			—
	4.980	4.925					
	6.945	5.059					

mass ($m_b = 4.823\,\text{GeV}$) is obtained from Refs. [26, 35]. We obtained the mass of $b\bar{b}$ in two models. The classical model at $\alpha = \beta = 1$ with topological defect ($\lambda = 0.7$). We obtained a good result compared with previous works and some of the states of bottomonium that are close to experimental data. We calculated the total error that equals to 0.006% in the classical model which is smaller than previous works. In the fractional model ($\alpha = 0.8$, $\beta = 0.9$) at $\lambda = 0.8$, the total error is smaller than the classical model. The topological defect produces a splitting in the mass spectrum of the $b\bar{b}$ meson to break the degeneracy in the nP and nD states, which was not considered in earlier studies. In Ref. [36], they studied the N-radial Schrödinger equation by using the asymptotic iteration method for the quark-antiquark interaction potential, and they calculated the mass spectra of heavy quarkonia. We found the total error of this research which equals to 0.484%. In Ref. [38], the authors calculated the N-radial Schrödinger equation by using the power series iteration method for the quark-antiquark interaction potential, and they calculated the mass spectra of heavy quarkonia. We calculated the total error of this work that equals to 0.0137%. In Ref. [40], the authors studied the N-radial Schrödinger equation by using the asymptotic iteration method with the Cornell potential, and

Table 4: Expectation value of charmonium of $\langle y^{-1} \rangle$ (GeV) for two models (the classical model ($\alpha = \beta = 1$, $\lambda = 0.15$), the fractional model ($\alpha = 0.59$, $\beta = 0.2$, $\lambda = 0.6$)).

State	The classical model $\langle y^{-1} \rangle$ (GeV)	The fractional model $\langle y^{-1} \rangle$ (GeV)	[44]	[44]	[45]	[46]
1S	1.173	0.502	0.456	0.454	0.492	0.507
2S	0.805	0.268	0.251	0.250	0.325	0.396
1P	0.342	0.308	0.312	0.312	—	0.316
	0.795	0.393				
	0.276	0.485				
2P	0.319	0.197	0.188	0.188	0.307	0.239
	0.628	0.231				
	0.263	0.262				
1D	0.226	0.442	0.202	0.203	—	
	0.396	0.347				
	0.562	0.275				
	0.254	0.224				
	0.184	0.189				

Table 5: Expectation value of bottomonium of $\langle y \rangle$ ($(\text{GeV})^{-1}$) for two models (the classical model ($\alpha = \beta = 1$, $\lambda = 0.13$), the fractional model ($\alpha = 0.7$, $\beta = 0.1$, $\lambda = 0.6$)).

State	The classical model $\langle y \rangle$ ($(\text{GeV})^{-1}$)	The fractional model $\langle y \rangle$ ($(\text{GeV})^{-1}$)	[44]	[44]	[45]	[46]
1S	0.600	1.874	1.615	1.556	1.823	1.574
2S	0.819	2.785	2.887	2.736	3.100	2.523
1P	1.861	1.888	2.105	1.981	—	2.306
	0.794	1.983				
	2.218	2.140				
2P	1.974	2.796	3.551	3.309	2.446	3.017
	0.980	2.880				
	2.318	3.019				
1D	2.790	1.925	2.956	2.732	—	—
	1.666	2.056				
	1.058	2.231				
	2.382	2.428				
	3.226	2.634				

we found the total error in the results which equals to 0.028%. Therefore, we obtained improved results in comparison with [36, 38, 40].

In Figure 1, the levels are different from the Minkowski levels, at $m = 1$ of P-states of charmonium. In Figure 1(a), we note that the splitting increases as λ decreases compared to Figure 1(b). This finding is in agreement with Ref. [41]. In addition, we note that the effect of different values of α, $\beta < 1$ also appeared on the splitting. Since $\lambda < 1$, the degenerated levels appear.

In Figure 2, we note the P-states of charmonium when $m = 0$. The topological defect does not affect the system and no splitting appears. This is in agreement with Ref. [41], but the generalized fractional parameter plays a role where in Figure 2(a), we take $\alpha = \beta = 0.9$ and in Figure 2(b) $\alpha = \beta = 0.4$. We note that in Figure 2(b), the curve is higher than the curve in Figure 2(a).

In Figure 3, we observe the P-states of charmonium when $m = -1$. Since complex eigenenergy appears by the negative sign of m_l, some states do not see it. This is in agreement with Ref. [41]. Also, the generalized fractional parameter plays a role where in Figure 3(a), we take $\alpha = \beta = 0.9$ and in Figure 3(b) $\alpha = \beta = 0.4$. We note that in Figure 3(b), the curve is higher than the curve in Figure 3(a).

In Figure 4, the levels are different from the Minkowski levels, as we can see with $m = 1$ of P-states of bottomonium. In Figure 4(a), we note that the splitting increases as λ decreases compared to Figure 4(b) since we took $\lambda = 0.4$ in Figure 4(a) and $\lambda = 0.8$ in Figure 4(b). This is in agreement with Ref. [41]. We note that fractional parameters

Table 6: Expectation value of bottomonium of $\langle y^{-1} \rangle$ (GeV) for two models (the classical model ($\alpha = \beta = 1$, $\lambda = 0.2$), the fractional model ($\alpha = 0.56$, $\beta = 0.1$, $\lambda = 0.5$)).

State	The classical model $\langle y^{-1} \rangle$ (GeV)	The fractional model $\langle y^{-1} \rangle$ (GeV)	[44]	[44]	[45]	[46]
1S	2.352	0.847	0.848	0.874	0.686	0.8706
2S	1.593	0.478	0.493	0.518	0.486	0.6946
1P	0.847	0.844				
	1.565	0.770	0.632	0.668	—	0.467
	0.614	0.658				
2P	0.759	0.447				
	1.226	0.452	0.393	0.420	0.467	0.4421
	0.573	0.410				
1D	0.548	0.835				
	1.083	0.745				
	1.083	0.634	0.435	0.469		
	0.548	0.538				
	0.398	0.464				

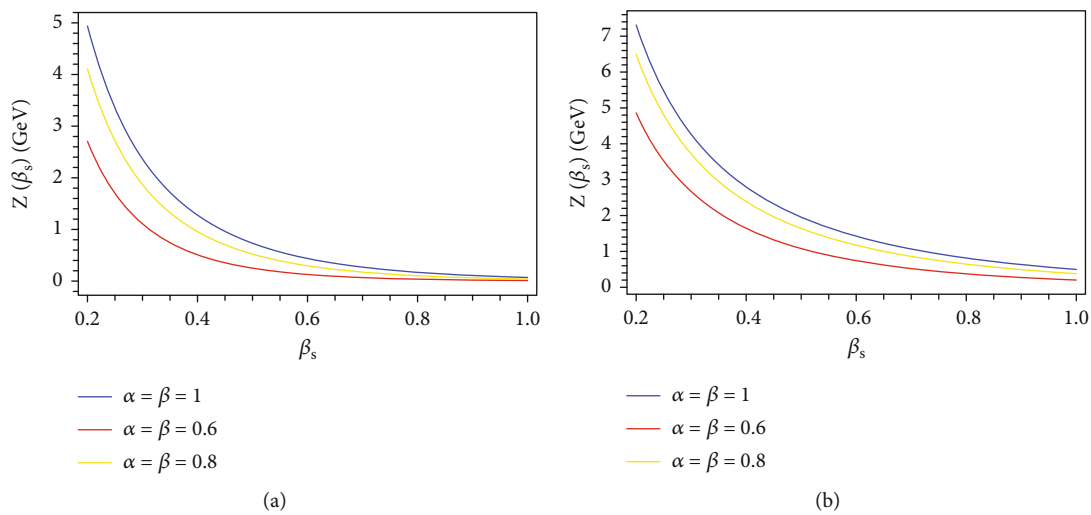

Figure 7: (a) The partition function (Z) for the second excited states of $c\bar{c}$ is shown as a function of β_s, for different values of α and β with $l = 1$ and $m_l = +1$ at topological defect ($\lambda = 0.2$). (b) The partition function (Z) for the second excited states of $c\bar{c}$ is shown as a function of β_s, for different values of α and β with $l = 1$ and $m_l = +1$ at topological defect ($\lambda = 0.8$).

act on the splitting mass where the degenerated levels appear.

In Figure 5, we note the P-states of bottomonium when $m = 0$. The topological defect does not affect the system and no splitting appears. This is in agreement with Ref. [41], but the generalized fractional parameter plays a role where in Figure 5(a), we take $\alpha = \beta = 0.9$ and in Figure 5(b) $\alpha = \beta = 0.4$. We note that in Figure 5(b), the splitting mass is higher than its values in Figure 5(a). In Figure 6, at $m = -1$, the P-states of bottomonium were noted. Some states do not see this since complex eigenvalues of energy appear by the negative sign of m_l. This is in agreement with Ref. [41]. Also, the generalized fractional parameter plays a role where in Figure 6(a), we take $\alpha = \beta = 0.9$ and in Figure 6(b) $\alpha = \beta = 0.4$. We note that in Figure 6(b), the splitting mass is higher than its values in Figure 6(a).

4.3. The Radial Expectation Values. The radial expectation values were given by the relation

$$\langle y^g \rangle = \int_0^\infty y^g |\psi_{nl}(y)|^2 dy. \tag{42}$$

In Table 3, the radial mean value $\langle y \rangle$ ($(\text{GeV})^{-1}$) for various levels of charmonium and topological defect causes to split nP and nD states. The mean values were calculated with the normalized wave function in two cases (first case ($\alpha = \beta = 1$, $\lambda = 0.1$)). The result in this case is acceptable with other works. In the second case ($\alpha = 0.6$, $\beta = 0.27$, $\lambda = 0.9$), the generalized fractional parameter plays an important role where the results are in agreement with other works [44–47].

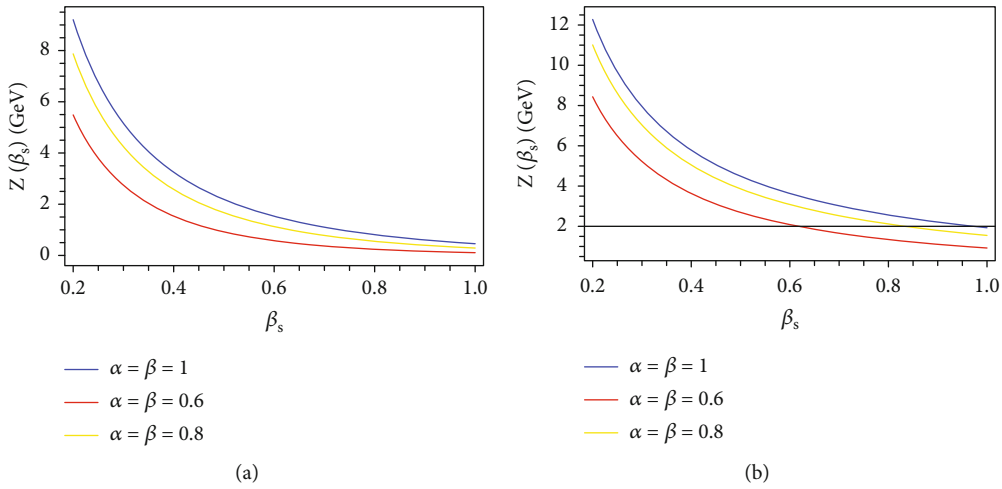

FIGURE 8: (a) The partition function (Z) for the second excited states of $b\bar{b}$ is shown as a function of β_s, for different values of α and β with $l = 1$ and $m_l = +1$ at topological defect ($\lambda = 0.2$). (b) The partition function (Z) for the second excited states of $c\bar{c}$ is shown as a function of β_s, for different values of α and β with $l = 1$ and $m_l = +1$ at topological defect ($\lambda = 0.8$).

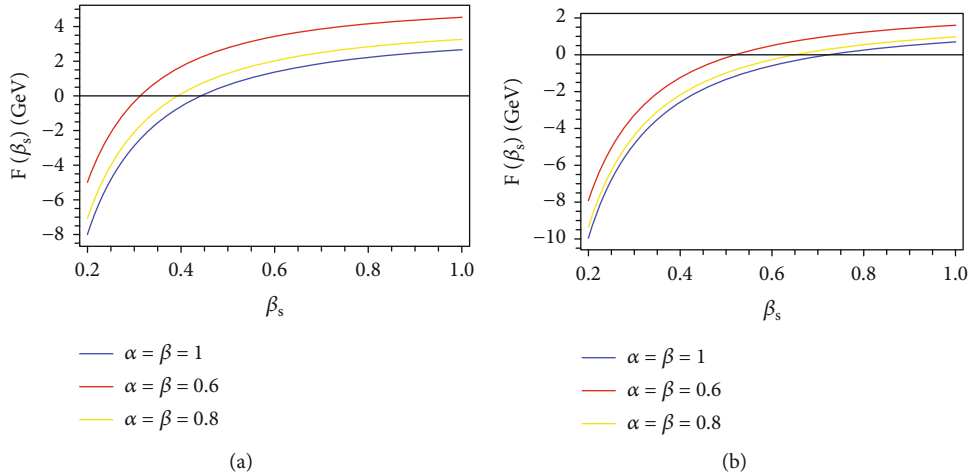

FIGURE 9: (a) The free energy plotted for the second excited states of $c\bar{c}$ is shown as a function of β_s, for different values of α and β with $l = 1$ and $m_l = +1$ at topological defect ($\lambda = 0.2$). (b) The free energy for the second excited states of $c\bar{c}$ is shown as a function of β_s, for different values of α and β with $l = 1$ and $m_l = +1$ at topological defect ($\lambda = 0.8$).

In Table 4, the radial mean value $\langle y^{-1} \rangle$ (GeV) for various levels of charmonium and topological defect causes to split nP and nD states. The mean value was calculated with the normalized wave function in two models: the classical model ($\alpha = \beta = 1$, $\lambda = 0.15$) and the fractional model ($\alpha = 0.59$, $\beta = 0.2$, $\lambda = 0.6$). The present results are in agreement with other works [44–47]. In Table 5, the radial mean value $\langle y \rangle$ ((GeV)$^{-1}$) for various levels of bottomonium and topological defect causes to split nP and nD states. The mean value was calculated using the normalized wave function in two models ($\alpha = \beta = 1$, $\lambda = 0.13$); we note that the effect of the topological defect on S-states does not appear like P-states and D-states. In the fractional model ($\alpha = 0.7, \beta = 0.1$, $\lambda = 0.6$), the generalized fractional parameter plays an important role especially in S-states and P-states and D-states where the results are in agreement with other works [44–46]. Also, we can see that the average value $\langle y \rangle$ ((GeV)$^{-1}$) decreases for bottomonium with an increase in the reduced mass compared with charmonium. In Table 6, the radial mean value $\langle y^{-1} \rangle$ (GeV) for various levels of bottomonium and topological defect causes to split nP and nD states. The mean values were calculated with the normalized wave function in the classical and fractional models. In the classical model ($\alpha = \beta = 1$, $\lambda = 0.13$), we note that the effect of topological defect on S-states does not appear like P-states and D-states; the results in this model are in good agreement with other works [4, 44, 45]. In the fractional model ($\alpha = 0.7, \beta = 0.1, \lambda = 0.6$), the generalized fractional parameter plays an important role especially in S-states and P-states and D-states. In addition, the results increase for bottomonium compared with charmonium.

4.4. Thermodynamic Properties of Heavy Quarkonia. The partition function serves as the foundation for thinking about the thermodynamic properties of heavy quarkonia

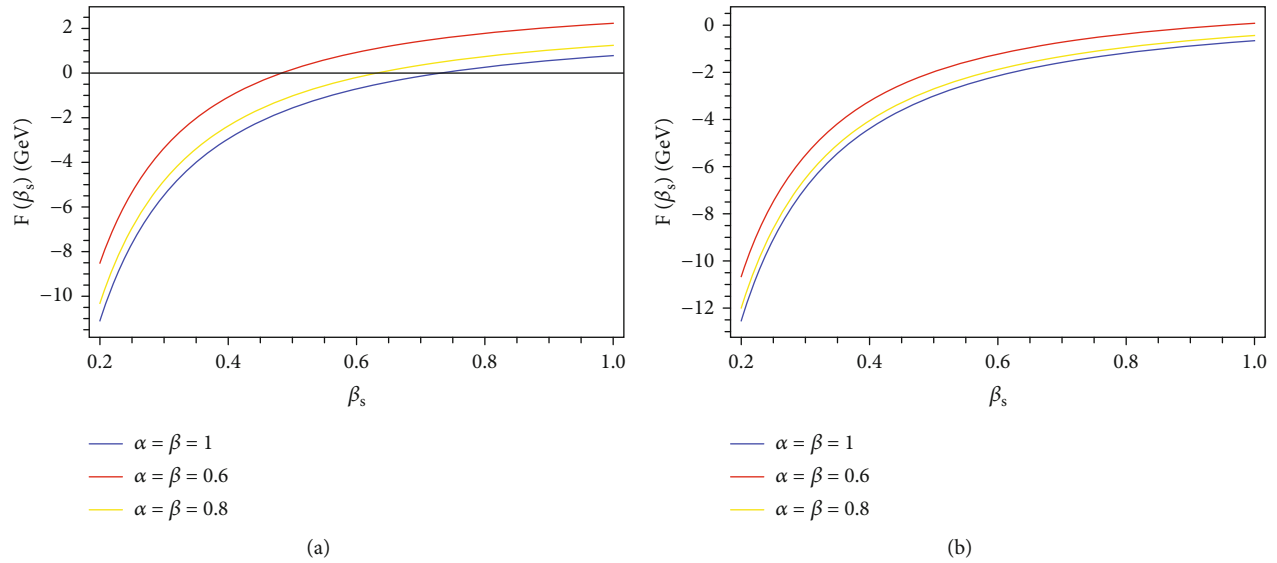

FIGURE 10: (a) The free energy plotted for the second excited states of $b\bar{b}$ is shown as a function of β_s, for different values of α and β with $l = 1$ and $m_l = +1$ at topological defect ($\lambda = 0.2$). (b) The free energy for the second excited states of $c\bar{c}$ is shown as a function of β_s, for different values of α and β with $l = 1$ and $m_l = +1$ at topological defect ($\lambda = 0.8$).

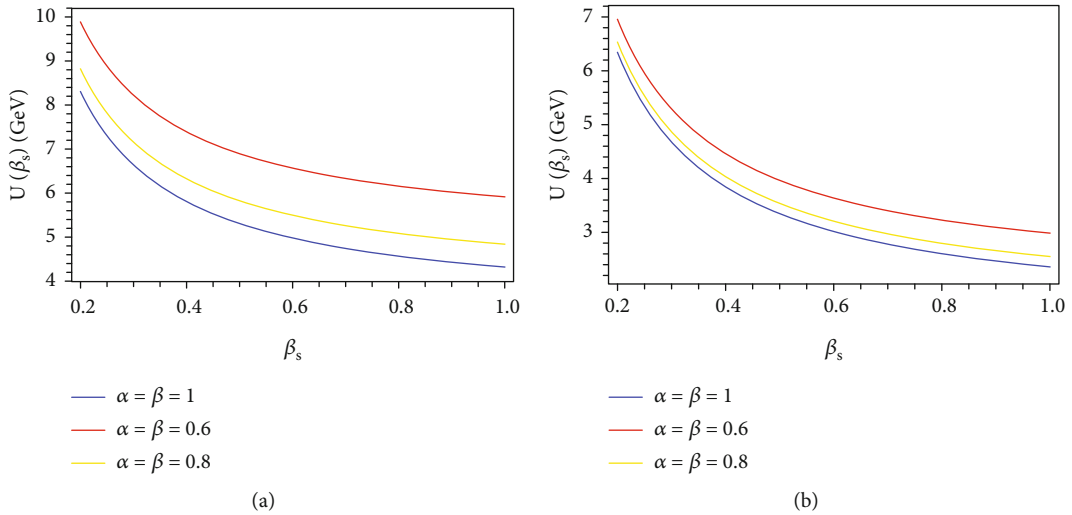

FIGURE 11: (a) The mean energy plotted for the second excited states of $c\bar{c}$ is shown as a function of β_s, for different values of α and β with $l = 1$ and $m_l = +1$ at topological defect ($\lambda = 0.2$). (b) The mean energy for the second excited states of $c\bar{c}$ is shown as a function of β_s, for different values of α and β with $l = 1$ and $m_l = +1$ at topological defect ($\lambda = 0.8$).

inside the cosmic string framework [48, 49]. According to statistical mechanics, the partition function can be built as follows.

4.4.1. Partition Function.

$$Z(\beta_s) = \sum_{n=0}^{\infty} e^{-\beta_s E_n} = \frac{1}{2} e^{-\beta_s \left[d - \left(b^2/4\,a\right) + \zeta^2 \sqrt{2a/M} \left[\alpha + \sqrt{(\alpha^2/4) + \left(1/\zeta^2\right)[l - (1 - (1/\lambda))m][l - (1 - (1/\lambda))m + 1]}\right]\right]} \operatorname{Csch}\left[\frac{\alpha}{2}\beta_s \zeta^2 \sqrt{\frac{2a}{M}}\right], \tag{43}$$

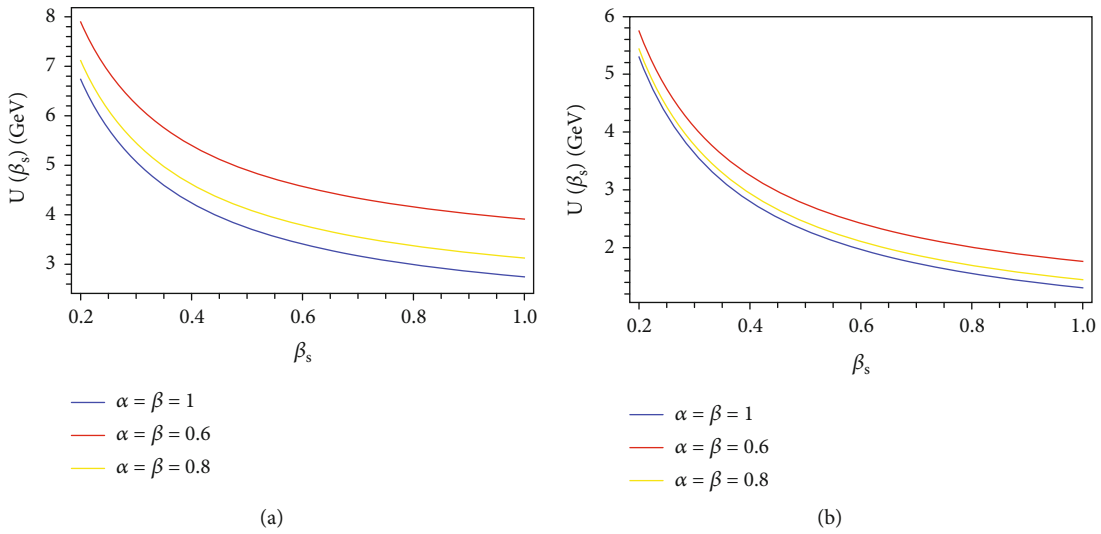

FIGURE 12: (a) The mean energy plotted for the second excited states of $b\bar{b}$ is shown as a function of β_s, for different values of α and β with $l = 1$ and $m_l = +1$ at topological defect ($\lambda = 0.2$). (b) The mean energy for the second excited states of $b\bar{b}$ is shown as a function of β_s, for different values of α and β with $l = 1$ and $m_l = +1$ at topological defect ($\lambda = 0.8$).

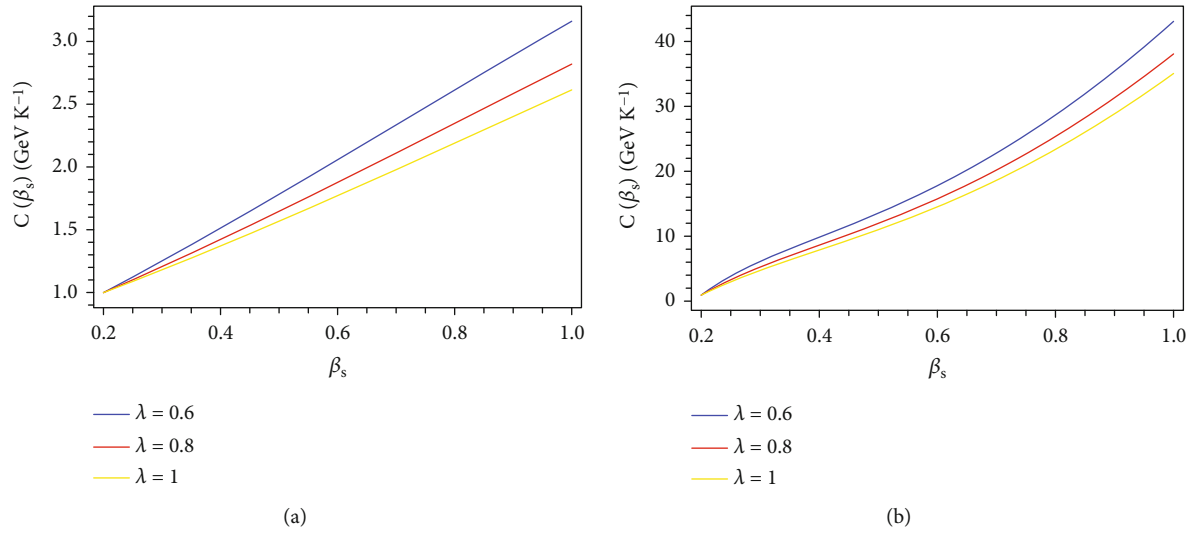

FIGURE 13: (a) The specific heat plotted for the second excited states of $c\bar{c}$ is shown as a function of β_s, for different values of topological defect at $\alpha = \beta = 0.8$ with $l = 1$ and $m_l = +1$. (b) The specific heat plotted for the second excited states of $c\bar{c}$ is shown as a function of β_s, for different values of topological defect at $\alpha = \beta = 0.1$ with $l = 1$ and $m_l = +1$.

where $\beta_s = 1/K\,T$, the Boltzmann constant is K, and the system's absolute temperature is T.

In Figures 7 and 8, we plot the partition function of P-states of charmonium and bottomonium as a function of β_s at different values from α, β under the effect of topological defect. We note that by increasing the values of α, β, the curve becomes higher. In Figures 7(a) and 8(a), we take the topological defect $\lambda = 0.2$. We note that the curves are not connected to the standard Minkowski curve, and we also note that the splitting increases as λ decreases which is in agreement with [50–52] and $Z(\beta_s)$ decreases with increasing β_s which is in agreement with [50]. The authors of [51] within the framework of the NU approach have used DFDEP to solve the Klein-Gordon equation, and they obtained the energy eigenvalues and associated wave function in D dimensions in great detail and noticed that the $Z(\beta)$ for the Minkowskian case monotonically lowers with increasing β. In Ref. [52], the partition function Z decreases monotonically with increasing λ for the two diatomic molecules considered and reaches a constant value for some typical values of λ. In Ref. [53], the author plotted the partition function of P-states of charmonium and bottomonium as a function of β_s at different values of topological defect, and they show that by increasing the topological defect, $Z(\beta)$ decreases with increasing β. In Ref. [50], based on the generalized Dunkl derivative in quantum mechanics, we study the one-dimensional Schrödinger equation with a harmonic oscillator potential and obtain the energy eigenvalues. For

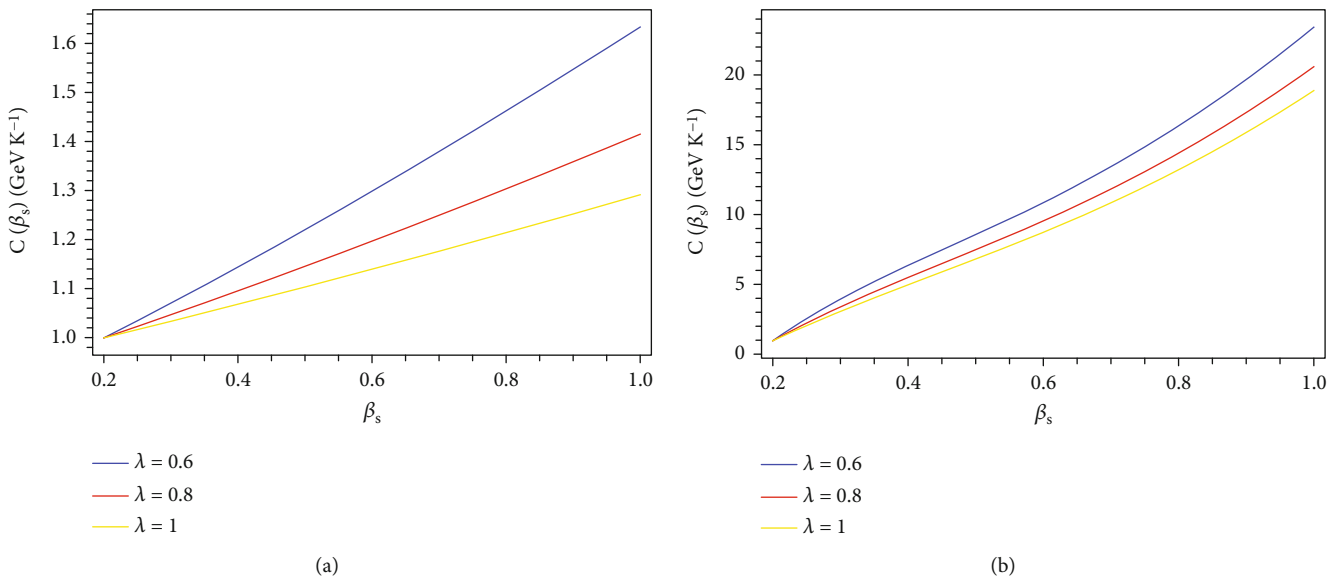

FIGURE 14: (a) The specific heat plotted for the second excited states of $b\bar{b}$ is shown as a function of β_s, for different values of topological defect at $\alpha = \beta = 0.8$ with $l = 1$ and $m_l = +1$. (b) The specific heat plotted for the second excited states of $b\bar{b}$ is shown as a function of β_s, for different values of topological defect at $\alpha = \beta = 0.1$ with $l = 1$ and $m_l = +1$.

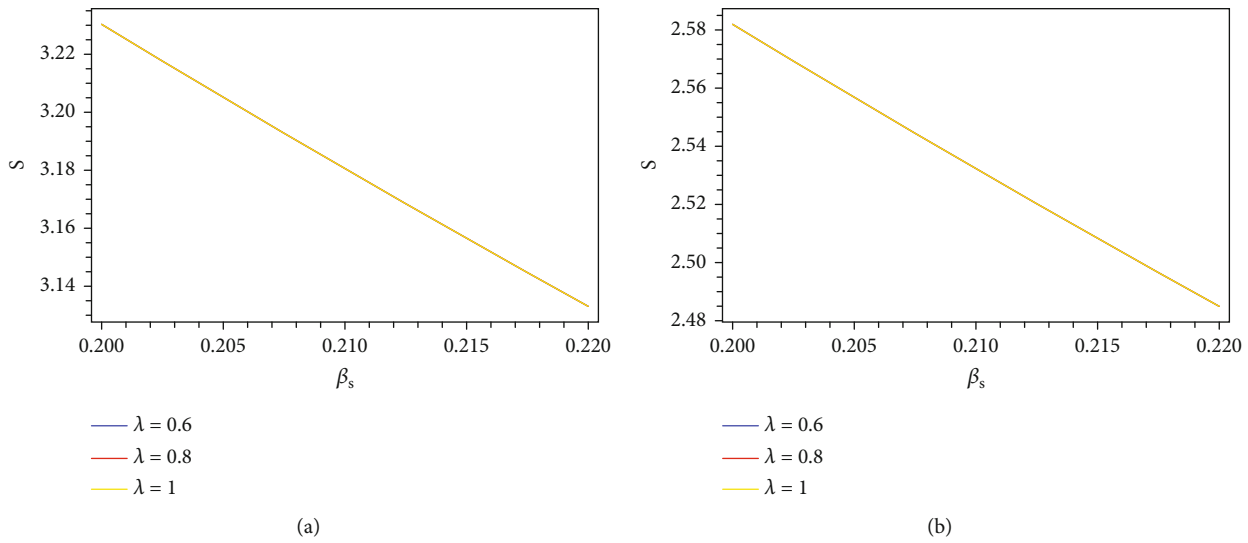

FIGURE 15: (a) The entropy plotted for the second excited states of $c\bar{c}$ is shown as a function of β_s, for different values of topological defect at $\alpha = \beta = 0.9$ with $l = 1$ and $m_l = +1$. (b) The entropy plotted for the second excited states of $c\bar{c}$ is shown as a function of β_s, for different values of topological defect at $\alpha = \beta = 0.4$ with $l = 1$ and $m_l = +1$.

the principal thermodynamic properties, they obtain that the $Z(\beta)$ decreases with β_s. In Figures 9 and 10, we plot the free energy of P-states of charmonium and bottomonium as a function of β_s at different values from α, β under the effect of topological defect. We note that with increasing the values of α, β, the curve becomes higher. In Figures 9(a) and 10(a), we took the topological defect $\lambda = 0.2$, and we note that the curves are not connected to the standard Minkowski curve. We note also that the splitting increases as λ decreases and free energy increases with increasing β_s, and we note that free energy (F) decreases by increasing the temperature. In Ref. [54], they show that F decreases by increasing the temperature of neutral particles. This is in agreement with [48, 49, 53, 54]. In Figures 11 and 12, we plot the mean energy of P-states of charmonium and bottomonium as a function of β_s at different values of α, β under the effect of topological defect. We note that by increasing the values of α, β, the curve becomes lower values. In Figures 11(a) and 12(a), we took the topological defect $\lambda = 0.2$ and note that the curves are separated from the classical Minkowski curve. We note also that the splitting increases as λ decreases and mean energy (U) decreases with increasing β_s, and with

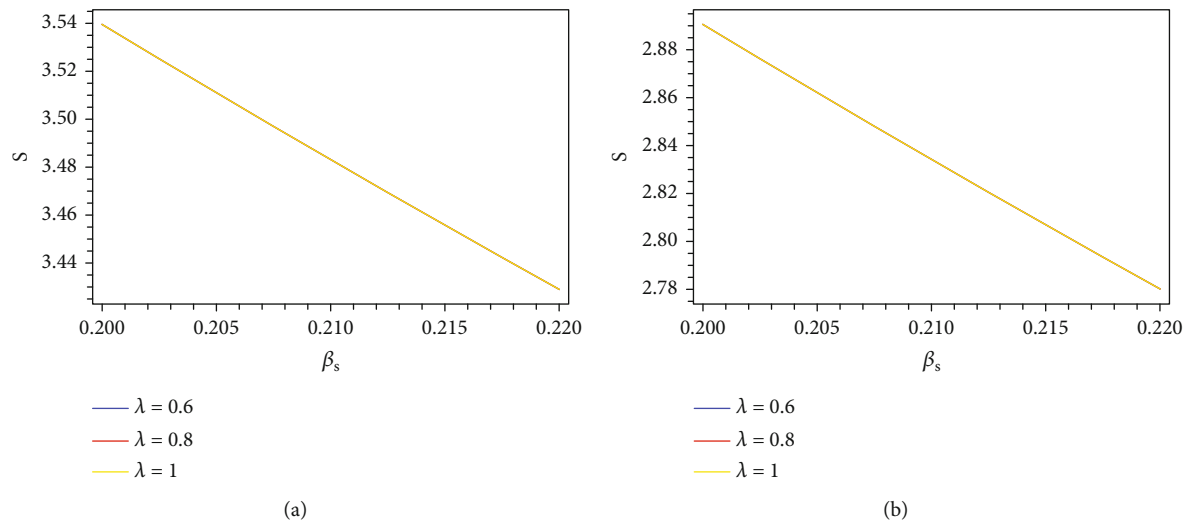

FIGURE 16: (a) The entropy plotted for the second excited states of $b\bar{b}$ is shown as a function of β_s, for different values of topological defect at $\alpha = \beta = 0.9$ with $l = 1$ and $m_l = +1$. (b) The entropy plotted for the second excited states of $b\bar{b}$ is shown as a function of β_s, for different values of topological defect at $\alpha = \beta = 0.4$ with $l = 1$ and $m_l = +1$.

increasing the parameter of the topological defect, its values shift to lower values. In Ref. [54], they calculated the thermodynamic properties of neutral particles under the effect of topological defect from the nonrelativistic Schrödinger-Pauli equation. The authors noted that by increasing the temperature, U increases. In Ref. [55], the authors applied their proposed proper quantization rule to obtain the energy spectrum of the modified Rosen-Morse potential. The beauty and symmetry of this proper rule come from its meaning whenever the number of the nodes of $\varphi(x)$ or the number of the nodes of the wave function $\psi(x)$ increases by one; the momentum integral $\int x\,Bx\,A\,k(x)dx$ will increase by π. Based on this new approach, they present a vibrational high-temperature partition function to study thermodynamic functions and they found that mean energy (U) decreases with increasing β_s. In Ref. [50], the authors found that the mean energy (U) decreases with increasing β_s. This is in agreement with [50–55]. In Figures 13 and 14, we plot the specific heat (C) of P-states of charmonium and bottomonium as a function of β_s at different values from topological defect under effect α, β. We note that with increasing the topological defect, the specific heat decreases. This is in agreement with [56]. In Figures 13(b) and 14(b), we take $\alpha = \beta = 0.1$. We note that by increasing α, β, the curves became lower as in Figures 13(a) and 14(a), and we note that the specific heat increases with temperature such that in Ref. [55]. In Figures 15 and 16, we plot the entropy (S) of P-states of charmonium and bottomonium as a function of β_s at different values from topological defect under effect α, β. We note that there is no influence by topological defect parameters like the solution of Minkowski space-time. This is in agreement with [53, 54]. In Figures 15(b) and 16(b), we take $\alpha = \beta = 0.4$. We note that by increasing α, β, the curves became lower as in Figures 15(a) and 16(a). We note that the entropy decreases with β_s. This is in agreement with [50, 55].

4.4.2. Free Energy F.

$$F(\beta_s) = -\frac{1}{\beta_s} \ln Z(\beta_s). \tag{44}$$

4.4.3. Mean Energy U.

$$U(\beta_s) = -\frac{\partial}{\partial(\beta_s)} \ln Z(\beta_s). \tag{45}$$

4.4.4. Specific Heat C.

$$C(\beta_s) = \frac{\partial(U)}{\partial T} = -K{\beta_s}^2 \frac{\partial(U)}{\partial(\beta_s)}. \tag{46}$$

4.4.5. The Entropy.

$$S(\beta_s) = K \ln Z(\beta_s) - K\beta_s \frac{\partial \ln Z(\beta_s)}{\partial \beta_s}. \tag{47}$$

5. Conclusion

In this paper, we solved the radial Schrödinger equation in the cosmic string with the extended Cornell potential by using a generalized fractional derivative of the extended Nikiforov-Uvarov (GFD-ENU) method under the effect of topological defect. We obtained eigenvalues of energy and wave functions of heavy quarkonia in the fractional model. Firstly, we obtained the special cases from the general model, and then, we calculated the mass of charmonium and bottomonium in the two models (the first case is the classical model and the second is the fractional model) under the effect of topological defect; it has been noted that the splitting between nP and nD states is caused by the presence of the topological defect. The excited states are split into $2l + 1$ components, suggesting that a topological defect's gravity field

interacts with energy levels in a way that is comparable to the Zeeman effect brought on by the magnetic field where the results are close with experimental data and in good agreement with other works such as Refs. [36–40]. We note that generalized fractional derivative plays an important role in this work since we obtain lower total error in calculating the mass of heavy quarkonia. As we noted from Tables 1 and 2, the states of S are in very good agreement with experimental data; in particular, 1S state is close with the data. Also, the states 1P, 2P, and 1D are in very good agreement with the data. We also obtained the wave function; then, we calculated the root mean of charmonium and bottomonium in two models under the effect of topological defect, and the results are in agreement with Refs. [44–47]. The mass and thermodynamic properties were analyzed graphically. Concerning the classical limit, the thermodynamic quantities exhibit a shift. When the cosmic string parameter is low, this fluctuation becomes more important. Free energy increases with increasing β_s and we note that free energy decreases by increasing temperature; we note also that the splitting increases as λ decreases, and this is in agreement with Refs. [48, 49, 53, 54]. By increasing the values of α, β, the curve becomes higher. The $Z(\beta_s)$ shifts to lower values as λ decreases; this is in agreement with Refs. [51–53], and by increasing the values of α, β, the curve becomes higher values. The Minkowski curve is separated from the curves with $\lambda \neq 1$; then, by raising the λ, the mean energy values are changed to lower values. This is in agreement with Refs. [50–55]. By increasing α, β, the curves became lower. We note that by increasing the topological defect, the specific heat decreases; this is in agreement with [56]. Also, by increasing α, β, the curves became lower. We note that there is no influence by topological parameters on the entropy, and this is in agreement with [53, 54]. By increasing α, β, the curves became higher values. We hope to extend this work to include spin-spin, spin-orbital, and tensor interactions in future work.

Data Availability

All data are included in the manuscript.

Ethical Approval

The authors declare that they comply with ethical standards regarding the content of this paper.

Disclosure

The version of the work has been submitted [57].

Conflicts of Interest

The authors declare that they have no conflicts of interest.

Acknowledgments

This work was supported by the Sponsoring Consortium for Open Access Publishing in Particle Physics.

References

[1] M. Abu-Shady, "Chiral logarithmic quark model of N and Δ with an A-term in the mean-field approximation," *International Journal of Modern Physics A*, vol. 26, no. 2, pp. 235–249, 2011.

[2] M. Abu-Shady and E. M. Khokha, "Bound state solutions of the Dirac equation for the generalized Cornell potential model," *International Journal of Modern Physics A*, vol. 36, no. 29, article 2150195, 2021.

[3] M. Rashdan, M. Abu-Shady, and T. S. T. Ali, "Extended linear sigma model in higher order mesonic interactions," *International Journal of Modern Physics E*, vol. 15, no. 1, pp. 143–152, 2006.

[4] M. Abu-Shady and H. M. Mansour, "Quantized linear σ model at finite temperature, and nucleon properties," *Physical Review C: Nuclear Physics*, vol. 85, no. 5, 2012.

[5] M. Abu-Shady and S. Y. Ezz-Alarab, "Conformable fractional of the analytical exact iteration method for heavy quarkonium masses spectra," *Few-Body Systems*, vol. 62, no. 2, pp. 1–8, 2021.

[6] M. Abu-Shady, "The effect of finite temperature on the nucleon properties in the extended linear sigma model," *International Journal of Modern Physics E*, vol. 21, no. 6, article 1250061, 2012.

[7] M. Abu-Shady and M. Soleiman, "The extended quark sigma model at finite temperature and baryonic chemical potential," *Physics of Particles and Nuclei Letters*, vol. 10, no. 7, pp. 683–692, 2013.

[8] M. Abu-Shady, H. M. Mansour, and A. I. Ahmadov, "Dissociation of quarkonium in hot and dense media in an anisotropic plasma in the nonrelativistic quark model," *Advances in High Energy Physics*, vol. 2019, Article ID 4785615, 10 pages, 2019.

[9] T. W. B. Kibble, "Topology of cosmic domains and strings," *Journal of Physics A: Mathematical and General*, vol. 9, no. 8, p. 1387, 1976.

[10] A. Vilenkin and E. P. S. Shellard, *Cosmic Strings and Other Topological Defects*, Cambridge University Press, 1994.

[11] A. C. Davis and T. W. B. Kibble, "Fundamental cosmic strings," *Contemporary Physics*, vol. 46, no. 5, pp. 313–322, 2005.

[12] T. W. Kibble, G. Lazarides, and Q. Shafi, "Walls bounded by strings," *Physical Review D*, vol. 26, no. 2, pp. 435–439, 1982.

[13] J. Rocher, *Contraintes cosmologiques sur la physique de l'univers primordial*, Université Paris Sud-Paris XI, 2005.

[14] J. Audretsch and A. Economou, "Conical bremsstrahlung in a cosmic-string spacetime," *Physical Review D*, vol. 44, no. 12, pp. 3774–3785, 1991.

[15] D. D. Harari and V. D. Skarzhinsky, "Pair production in the gravitational field of a cosmic string," *Physics Letters B*, vol. 240, no. 3-4, pp. 322–326, 1990.

[16] W. Florkowski, *Phenomenology of Ultra-Relativistic Heavy-Ion Collisions*, World Scientific Publishing Company, 2010.

[17] U. Kakade and B. K. Patra, "Quarkonium dissociation at finite chemical potential," *Physical Review C*, vol. 92, no. 2, article 024901, 2015.

[18] T. Matsui and H. Satz, "J/ψ suppression by quark-gluon plasma formation," *Physics Letters B*, vol. 178, no. 4, pp. 416–422, 1986.

[19] V. S. Filinov, M. Bonitz, Y. B. Ivanov, E. M. Ilgenfritz, and V. E. Fortov, "Thermodynamics of the quark gluon plasma at finite

chemical potential: color path integral Monte Carlo results," *Contributions to Plasma Physics*, vol. 55, no. 2-3, pp. 203–208, 2015.

[20] M. Schleif and R. Wünsch, "Thermodynamic properties of the SU (2) f chiral quark–loop soliton," *The European Physical Journal A-Hadrons and Nuclei*, vol. 1, no. 2, pp. 171–186, 1998.

[21] M. Abu-Shady, "Meson properties at finite temperature in the linear sigma model," *International Journal of Theoretical Physics*, vol. 49, no. 10, pp. 2425–2436, 2010.

[22] M.-C. Zhang, G.-H. Sun, and S.-H. Dong, "Exactly complete solutions of the Schrödinger equation with a spherically harmonic oscillatory ring-shaped potential," *Physics Letters A*, vol. 374, no. 5, pp. 704–708, 2010.

[23] M. G. Miranda, G.-H. Sun, and S.-H. Dong, "The solution of the second Pöschl–Teller like potential by Nikiforov–Uvarov method," *International Journal of Modern Physics E*, vol. 19, no. 1, pp. 123–129, 2010.

[24] A. F. Nikiforov and V. B. Uvarov, *Special Functions of Mathematical Physics. Vol. 205*, Birkhäuser, Basel, 1988.

[25] H. Karayer, D. Demirhan, and F. Büyükkılıç, "Extension of Nikiforov-Uvarov method for the solution of Heun equation," *Journal of Mathematical Physics*, vol. 56, no. 6, 2015.

[26] M. Abu-Shady, "Quarkonium masses in a hot QCD medium using conformable fractional of the Nikiforov–Uvarov method," *International Journal of Modern Physics A*, vol. 34, no. 31, article 1950201, 2019.

[27] M. Abu-Shady, E. M. Khokha, and T. A. Abdel-Karim, "The generalized fractional NU method for the diatomic molecules in the Deng–Fan model," *The European Physical Journal D*, vol. 76, no. 9, p. 159, 2022.

[28] M. Abu-Shady and M. K. A. Kaabar, "A generalized definition of the fractional derivative with applications," *Mathematical Problems in Engineering*, vol. 2021, Article ID 9444803, 9 pages, 2021.

[29] M. O. Katanaev and I. V. Volovich, "Theory of defects in solids and three-dimensional gravity," *Annals of Physics*, vol. 216, no. 1, pp. 1–28, 1992.

[30] C. Furtado and F. Moraes, "On the binding of electrons and holes to disclinations," *Physics Letters A*, vol. 188, no. 4-6, pp. 394–396, 1994.

[31] B. Kumar, M. B. Paranjape, and U. A. Yajnik, "Fate of the false monopoles: induced vacuum decay," *Physical Review D*, vol. 82, no. 2, article 025022, 2010.

[32] B. H. Lee, W. Lee, R. MacKenzie, M. B. Paranjape, U. A. Yajnik, and D. H. Yeom, "Battle of the bulge: decay of the thin, false cosmic string," *Physical Review D*, vol. 88, no. 10, article 105008, 2013.

[33] L. Bergström and A. Goobar, *Cosmology and Particle Astrophysics*, Springer Science & Business Media, 2006.

[34] E. P. Inyang, A. N. Ikot, I. O. Akpan, J. E. Ntibi, E. Omugbe, and E. S. William, "Analytic study of thermal properties and masses of heavy mesons with quarkonium potential," *Results in Physics*, vol. 39, article 105754, 2022.

[35] A. Atangana Likéné, J. M. Ema'a Ema'a, P. Ele Abiama, and G. H. Ben-Bolie, "Nonrelativistic quark model for mass spectra and decay constants of heavy-light mesons using conformable fractional derivative and asymptotic iteration method," *International Journal of Modern Physics A*, vol. 37, no. 35, article 2250229, 2022.

[36] R. Kumar and F. Chand, "Asymptotic study to the N-dimensional radial Schrödinger equation for the quark-antiquark system," *Communications in Theoretical Physics*, vol. 59, no. 5, pp. 528–532, 2013.

[37] N. V. Maksimenko and S. M. Kuchin, "Determination of the mass spectrum of quarkonia by the Nikiforov–Uvarov method," *Russian Physics Journal*, vol. 54, no. 1, pp. 57–65, 2011.

[38] R. Kumar and F. Chand, "Series solutions to the N-dimensional radial Schrödinger equation for the quark–antiquark interaction potential," *Physica Scripta*, vol. 85, no. 5, article 055008, 2012.

[39] M. Abu-Shady and S. Y. Ezz-Alarab, "Trigonometric Rosen–Morse potential as a quark–antiquark interaction potential for meson properties in the non-relativistic quark model using EAIM," *Few-Body Systems*, vol. 60, no. 4, p. 66, 2019.

[40] R. Rani, S. B. Bhardwaj, and F. Chand, "Mass spectra of heavy and light mesons using asymptotic iteration method," *Communications in Theoretical Physics*, vol. 70, no. 2, p. 179, 2018.

[41] A. A. Likéné, D. N. Ongodo, J. M. E. Ema'a, P. E. Abiama, and G. H. Ben-Bolie, "Effects of gravitational field of a topological defect on heavy quarkonia spectra in a non-relativistic quark model," *Few-Body Systems*, vol. 64, no. 83, 2023.

[42] M. Tanabashi, P. D. Grp, K. Hagiwara, K. Hikasa, K. Nakamura, and Y. Sumino, "Review of particle physics," *Physical Review D*, vol. 98, no. 3, article 030001, 2018.

[43] R. M. Barnnett, C. D. Carone, D. E. Groom, T. G. Trippe, and C. Amsler, "Review of particle physics," *Physical Review D*, vol. 541, 1996.

[44] E. Omugbe, E. P. Inyang, I. J. Njoku et al., "Approximate mass spectra and root mean square radii of quarkonia using Cornell potential plus spin-spin interactions," *Nuclear Physics A*, vol. 1034, article 122653, 2023.

[45] G. R. Boroun and H. Abdolmalki, "Variational and exact solutions of the wavefunction at origin (WFO) for heavy quarkonium by using a global potential," *Physica Scripta*, vol. 80, no. 6, article 065003, 2009.

[46] P. Gupta and I. Mehrotra, "Study of heavy quarkonium with energy dependent potential," *Journal of Modern Physics*, vol. 3, no. 10, pp. 1530–1536, 2012.

[47] D. A. Ramírez Zaldívar, F. Guzmán, and D. Arrebato, "Charmonio: comparación entre modelos potenciales," *Nucleus*, vol. 63, pp. 9–11, 2018.

[48] M. Modarres and A. Mohamadnejad, "The thermodynamic properties of weakly interacting quark-gluon plasma via the one-gluon exchange interaction," *Physics of Particles and Nuclei Letters*, vol. 10, no. 2, pp. 99–104, 2013.

[49] M. Modarres and H. Gholizade, "Strange quark matter in the framework of one gluon exchange and density and temperature dependent particle mass models," *International Journal of Modern Physics E*, vol. 17, no. 7, pp. 1335–1355, 2008.

[50] S. H. Dong, W. H. Huang, W. S. Chung, P. Sedaghatnia, and H. Hassanabadi, "Exact solutions to generalized Dunkl oscillator and its thermodynamic properties," *Europhysics Letters*, vol. 135, no. 3, p. 30006, 2021.

[51] A. N. Ikot, B. C. Lutfuoglu, M. I. Ngwueke, M. E. Udoh, S. Zare, and H. Hassanabadi, "Klein-Gordon equation particles in exponential-type molecule potentials and their thermodynamic properties in D dimensions," *The European Physical Journal Plus*, vol. 131, no. 12, pp. 1–17, 2016.

[52] W. A. Yahya and K. J. Oyewumi, "Thermodynamic properties and approximate solutions of the ℓ-state Pöschl–Teller-type potential," *Journal of the Association of Arab Universities for Basic and Applied Sciences*, vol. 21, no. 1, pp. 53–58, 2016.

[53] A. Likéné, A. Zarma, D. Ongodo, J. M. E. A. Ema'a, P. Abiama, and G. Ben-Bolie, "Effects of gravitational field of a topological defect on statistical properties of heavy quark-antiquark systems," *East European Journal of Physics*, vol. 3, no. 3, pp. 129–141, 2022.

[54] H. Hassanabadi and M. Hosseinpour, "Thermodynamic properties of neutral particle in the presence of topological defects in magnetic cosmic string background," *The European Physical Journal C*, vol. 76, no. 10, pp. 1–7, 2016.

[55] S.-H. Dong and M. Cruz-Irisson, "Energy spectrum for a modified Rosen-Morse potential solved by proper quantization rule and its thermodynamic properties," *Journal of Mathematical Chemistry*, vol. 50, no. 4, pp. 881–892, 2012.

[56] C. O. Edet, P. O. Nwbabuzor, E. B. Ettah et al., "Magnetotransport and thermal properties of the Yukawa potential in cosmic string space-time," *Results in Physics*, vol. 39, article 105749, 2022.

[57] M. Abu-shady and H. M. Fath-Allah, "Properties and behaviors of heavy quarkonia: insights through fractional model and topological defects," 2023, https://arxiv.org/abs/2309.14310.